Acta Cryst. (1998). B**54**, 66–72

Experimental Electron-Density Study of 4-Cyanoimidazolium-5-olate at 120 K

RICCARDO BIANCHI,[a]* GIULIANA GERVASIO[b] AND GUIDO VISCARDI[c]

[a]*Centro CNR per lo Studio delle Relazioni tra Struttura e Reattivita' Chimica, via Golgi 19, I-20133 Milano, Italy,* [b]*Dipartimento di Chimica Inorganica, Chimica Fisica e Chimica dei Materiali, Universita' di Torino, via Giuria 7, I-10125 Torino, Italy, and* [c]*Dipartimento di Chimica Generale ed Organica Applicata, Universita' di Torino, via Giuria 7, I-10125 Torino, Italy. E-mail: bian@rs6.csrsrc.mi.cnr.it*

(*Received 11 June 1997; accepted 23 June 1997*)

Abstract

This paper presents an analysis of the electron density in 4-cyanoimidazolium-5-olate, determined by the rigid pseudoatom model from accurate X-ray data measured at 120 K. A comparison of the electrostatic potential between experiment and theory is given for the isolated molecule. The results confirm the typical mesoionic electron distribution of the title compound and the presence of three hydrogen bonds in the crystal structure. The atomic charges and molecular dipole moment derived from the *ab initio* Hartree–Fock method are close to those obtained from the multipole model, which includes the kappa radial parameters. Electrostatic energies are also calculated for hydrogen bonding and molecular stacking interactions.

1. Introduction

During the X-ray analysis at room temperature (293 K) of some imidazole derivatives (Barni *et al.*, 1997) we found a mesoionic molecule crystallized in a noncentrosymmetric space group, with high response to the SHG (second harmonic generation) measurements and with drug properties. Owing to the interesting features of this molecule, the electron-density distribution of the title compound, determined experimentally at 120 K by the multipole-expansion method (Stewart, 1976), is illustrated in the present paper. A topological analysis of the experimental density (Bader & Essén, 1984; Bader, 1990), performed in order to define uniquely the interactions occurring between its constituent atoms, is also considered together with the molecular electrostatic potential calculated by the multipole model and by the *ab initio* Hartree Fock (HF) method, using wavefunctions of different accuracy. Intermolecular electrostatic energies were finally computed, using a simple method proposed by Spackman (1986*a*,*b*, 1987). Our study mainly analyzes the covalent bonding and the N—H···O and C—H···N interactions in the present crystal structure.

2. Experimental

The present work employs a set of X-ray data collected at 120 K from a small crystal of 4-cyanoimidazolium-5-olate (1) of dimensions 0.12 × 0.08 × 0.30 mm. This compound crystallizes in the orthorhombic system with space group $Pna2_1$, a = 12.584 (3), b = 9.699 (2), c = 3.674 (2) Å, V = 448.4 (3) Å^3 and Z = 4, D_x = 1.616 g cm^{-3}, μ = 0.124 mm^{-1}. The measurements were made using a Siemens P4 diffractometer equipped with a low-temperature device (liquid nitrogen) and the data were collected in the 2θ range 2.0–80.0°, with scan type θ–2θ and a variable scan speed from 2.0 to 11.7° min^{-1}. The X-ray radiation was Mo $K\alpha$ (λ = 0.71073 Å); two standard reflections were measured every 50 reflections (the collected reflections were 2943). All calculations based on X-ray data were performed using a modified version of the *VALRAY* program (Stewart & Spackman, 1983).

2.1. *Structure refinement*

The quantity minimized in the refinements was $\Sigma w(|F_o|^2 - k^2|F_c|^2)^2$ based on 1528 independent reflections up to $\sin\theta/\lambda$ = 0.91 Å^{-1} and weights $w = 1/\sigma^2(F_o^2)$, with $\sigma(F_o^2)$ the s.u. of the square of the observed structure factor. Absorption, extinction corrections and anomalous dispersion were not considered. During each refinement, the scale factor k was estimated by the sum of the monopole populations divided by $F(000)$. The least-squares refinements were carried out on a number of different models; we describe three of them, IAM, POP and POPK, here.

2.1.1. *IAM.* The independent atom model (IAM) is the conventional model for the structure refinement. The scattering factors for C, N and O atoms were derived from the Hartree–Fock atomic functions tabulated by Clementi & Roetti (1974) and for H atoms from Slater-type atomic orbitals with standard molecular exponents (Hehre *et al.*, 1970).

2.1.2. *POP.* A multipole model, with the electron density of molecule (1) represented by an expansion in terms of rigid pseudoatoms (Stewart, 1976). Each pseudoatom is assigned a small finite multipole expansion of the atomic form factor (generalized scattering factor model or g.s.f. model) with a variable population parameter for each surface harmonic. The multipole expansion included two monopoles (one termed 'inner'

and the other 'outer') and the higher terms were up to the octopole level, except for H atoms (a monopole and a dipole). The monopoles on heavy atoms consist of shells constructed from the localized SCF (self-consistent field) s and p orbitals (Clementi & Roetti, 1974). Each H monopole was a single shell, given by $\exp(-2.48r)$. For the higher multipoles, exponential radial functions with fixed standard molecular exponents (Hehre *et al.*, 1970) were used for all atoms. The same 'inner' monopole parameter was assumed for all O, N and C atoms. The positions of the H atoms were fixed to those obtained by a multipole refinement, assuming the hydrogens polarized in the direction of the atom to which they are bonded. The thermal function was considered isotropic for hydrogens and anisotropic for the other atoms.

2.1.3. *POPK*. This is an extension of the POP multipole model, where the 'outer' monopoles of the heavy atoms were shaped with a variable scaling parameter, k, describing the contraction/expansion of the spherical component of the valence electron density (van der Wal & Stewart, 1984).

2.2. *X-ray properties*

The electron population of individual atoms was calculated, but it is model dependent and has limited physical significance. In the literature several schemes have been described for partitioning the total charge density distribution. If partitioning were carried out by means of the interatomic surfaces defined by Bader & Essén (1984) a more significant set of atomic populations would be obtained. However, the electron density is generally much smaller between molecules than it is between atoms of the same molecule. Therefore, when the charge distribution is partitioned into molecular components, the resulting estimates of molecular properties should be correspondingly less model dependent. It must also be remembered that pseudoatom parameters describe the molecule as it occurs in its crystal environment and consequently the parameters will incorporate the effects of molecular interactions including hydrogen bonding.

The total electron density, $\rho(r)$, based on g.s.f.'s, was calculated with a direct space lattice sum. The gradient of $\rho(r)$ and its Hessian were also computed with a direct space lattice sum. The topology of $\rho(r)$ can be fully described by its critical points, where the gradient of $\rho(r)$ vanishes (Bader & Essén, 1984). Critical points were located by the Newton–Raphson procedure in direct space. The molecular electrostatic potential was computed assuming the g.s.f.'s derived from the pseudoatom model.

The intermolecular energies were calculated with a model (Spackman, 1986*a*,*b*, 1987) in which the total energy is $E_{es} + E_{pen} + E_{rep} + E_{dip}$. The electrostatic and penetration energies (E_{es} and E_{pen}) are derived from the experimental charge density. The repulsion and dispersion energies (E_{rep} and E_{dip}) were approximated by a sum of atom–atom potentials.

2.3. *Ab initio properties*

For comparison purposes, atomic populations, the electrostatic potential and the dipole moment for an

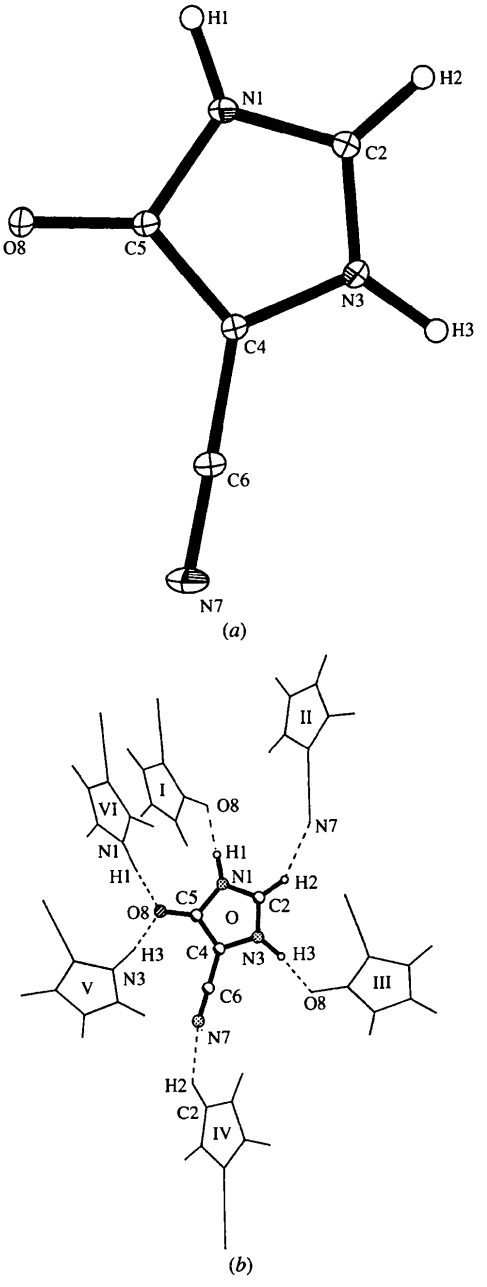

Fig. 1. (*a*) *ORTEP*II (Johnson, 1976) drawing of the molecular structure at 120 K. Ellipsoids are drawn at the 50% probability level. (*b*) Molecules (1) in the crystal connected by hydrogen bonds. Symmetry codes: (i) $-x, -y, -\frac{1}{2}+z$; (ii) $-\frac{1}{2}+x, \frac{1}{2}-y, -1+z$; (iii) $\frac{1}{2}-x, \frac{1}{2}+y, -\frac{1}{2}+z$; (iv) $\frac{1}{2}+x, \frac{1}{2}-y, 1+z$, (v) $\frac{1}{2}-x, -\frac{1}{2}+y, \frac{1}{2}+z$; (vi) $-x, -y, \frac{1}{2}+z$.

Table 1. *Refinement information*

	IAM	POP	POPK
N_o (Number of reflections)	1528	1528	1528
N_p (Number of parameters)	84	215	223
$S = [\Sigma w(\|F_o\|^2 - k^2\|F_c\|^2)^2/(N_o - N_p)]^{1/2}$	3.432	1.851	1.763
$wR(F^2) = [\Sigma w(\|F_o\|^2 - k^2\|F_c\|^2)^2/\Sigma w\|F_o\|^4]^{1/2}$	0.0732	0.0380	0.0358
$R(F^2) = \Sigma\|\|F_o\|^2 - k^2\|F_c\|^2\|/\Sigma\|F_o\|^2$	0.0663	0.0376	0.0357
k (scale factor)	1.001 (3)	1.005 (4)	0.994 (5)
$(\text{shift/s.u.})_{max}$	< 0.02	< 0.08	< 0.05

isolated molecule were also evaluated, using the experimental geometry (POPK model) and the *ab initio* Hartree–Fock method as implemented in the *Gaussian*92 program (Frisch *et al.*, 1992). The adopted basis sets were the standard 3-21G and 6-31G** basis.

3. Results and discussion

3.1. *Crystal structure*

The molecular structure of (1) is shown in Fig. 1(*a*). Fig. 1(*b*) shows the hydrogen bonds formed in the crystal by the three available protons of each molecule. Two of them involve the atom O8 and one involves N7. The molecules are packed along **c** and the crystal structure is stabilized by the N—H···O and C—H···N interactions among symmetry-related molecules. The final agreement factors and some other refinement information are listed in Table 1.† No relevant residual features are found in the difference Fourier synthesis after the POPK multipole refinement. Bond lengths and angles, along with hydrogen bonds are given in Tables 2 and 3, respectively. The bond distances and angles for heavy atoms, derived from the multipole models, are slightly different from those obtained from the independent atom model (IAM). However, the discrepancies are larger for the geometrical data involving H atoms. The N—H···O and C—H···N contacts calculated from the aspherical models are systematically shorter than the corresponding ones of the IAM model, thereby strengthening the role of hydrogen bonds in the crystal packing. In addition, the hydrogen bonds, reported in Table 3, show a significant reduction of the C2···N7 distance and a more linear N3—H3···O8 hydrogen bond on going from 293 to 120 K. These variations and the large contraction (31.5σ) of the c axis [c = 3.763 (2) Å at 293 K and c = 3.674 (2) Å at 120 K], due to strong van der Waals interactions involving π electrons among the imidazole rings faced along c, are the most relevant changes determined in the crystal packing by the temperature lowering.

† Lists of atomic coordinates, anisotropic displacement parameters, kappa and electronic parameters, and structure factors have been deposited with the IUCr (Reference: NA0081). Copies may be obtained through The Managing Editor, International Union of Crystallography, 5 Abbey Square, Chester CH1 2HU, England

Table 2. *Relevant bond distances (Å) and angles (°) from the conventional (IAM) and multipole refinements*

	IAM	POP	POPK
N1—C2	1.344 (2)	1.347 (2)	1.347 (2)
N1—C5	1.398 (2)	1.395 (2)	1.396 (2)
N1—H1	0.89 (1)	1.01 (1)	1.01 (1)
C2—N3	1.319 (2)	1.321 (1)	1.320 (2)
C2—H2	0.98 (2)	1.09 (2)	1.09 (2)
N3—C4	1.397 (2)	1.395 (2)	1.395 (2)
N3—H3	0.97 (2)	1.04 (2)	1.04 (2)
C4—C5	1.400 (1)	1.400 (1)	1.400 (1)
C4—C6	1.402 (2)	1.394 (2)	1.397 (2)
C5—O8	1.272 (2)	1.270 (2)	1.270 (2)
C6—N7	1.155 (2)	1.162 (2)	1.163 (2)
C2—N1—C5	110.3 (1)	110.02 (9)	110.03 (9)
C2—N1—H1	122.2 (7)	122.7 (9)	122.7 (9)
C5—N1—H1	127.2 (9)	126.9 (8)	126.8 (8)
N1—C2—N3	109.13 (9)	109.19 (8)	109.22 (8)
N1—C2—H2	125 (1)	125 (1)	125 (1)
N3—C2—H2	125.4 (8)	125.7 (7)	125.7 (7)
C2—N3—C4	108.59 (9)	108.55 (9)	108.51 (9)
C2—N3—H3	128.9 (8)	128.4 (7)	128.4 (7)
C4—N3—H3	122 (1)	123 (1)	123 (1)
N3—C4—C5	107.98 (9)	107.89 (8)	107.97 (8)
N3—C4—C6	123.3 (1)	123.15 (9)	123.13 (9)
C5—C4—C6	128.7 (1)	128.91 (8)	128.85 (8)
N1—C5—C4	104.00 (9)	104.35 (7)	104.26 (7)
N1—C5—O8	124.38 (9)	124.13 (8)	124.17 (8)
C4—C5—O8	131.62 (9)	131.52 (8)	131.56 (8)
C4—C6—N7	179.2 (1)	179.0 (1)	179.0 (1)

Table 3. *Hydrogen bonds and angles (Å, °)*

First-row IAM refinement at 293 K (Barni *et al.*, 1997); second-row IAM refinement at 120 K; third-row POP refinement at 120 K; fourth-row POPK refinement at 120 K.

D—H···*A*	H—*A*	*D*···*A*	*D*—H···*A*
N1—H1···O8^{i}	1.89 (2)	2.785 (2)	171 (3)
	1.90 (1)	2.781 (1)	176 (1)
	1.77 (2)	2.780 (1)	176 (1)
	1.77 (2)	2.780 (1)	176 (1)
C2—H2···N7^{ii}	2.30 (2)	3.167 (2)	145 (2)
	2.31 (2)	3.151 (2)	144 (1)
	2.20 (2)	3.151 (2)	145 (1)
	2.20 (2)	3.150 (2)	145 (1)
N3—H3···O8^{iii}	1.85 (2)	2.709 (2)	154 (2)
	1.75 (2)	2.704 (1)	168 (1)
	1.68 (2)	2.706 (1)	165 (1)
	1.68 (2)	2.706 (1)	165 (1)

(i) $-x, -y, -\frac{1}{2}+z$; (ii) $-\frac{1}{2}+x, \frac{1}{2}-y, -1+z$; (iii) $\frac{1}{2}-x, \frac{1}{2}+y, -\frac{1}{2}+z$.

3.2. *Electron density*

A point where the gradient of the electron density vanishes is defined as a critical point (CP). The nature of a CP is indicated by the pair (r,s), where r is the number of eigenvalues greater than zero and s is the difference between the number of positive and negative eigenvalues $(\lambda_1, \lambda_2, \lambda_3)$ of the Hessian matrix at the critical point. The (3,−3), (3,−1), (3,+1) and (3,+3) points are associated with nuclei, bonds, rings and cages of the molecular structure, respectively (Bader, 1990). The (3,−1) critical point, *i.e.* a bond critical point (BCP), is such that the density attains its minimum value along the bond path, a line connecting two nuclei where $\rho(\mathbf{r})$ is a maximum with respect to any lateral displacement from the line. It has been demonstrated (Bader & Essén, 1984) that atomic interactions fall into two broad general classes, closed-shell and shared interactions. Shared interactions (covalent and polar bonds) are characterized by large negative density curvatures in a direction perpendicular to the bond path with a negative Laplacian of the density at BCP, $\nabla^2\rho_b = \lambda_1 + \lambda_2, \lambda_3$. Closed-shell interactions (ionic bonds, van der Waals interactions and in most cases hydrogen bonds) are determined by dominance of the positive curvature λ_3, parallel to the bond path. The density value at the BCP, ρ_b, can be related to the bond order, $n = \exp[A(\rho_b - B)]$, where A and B depend on basis set (Cremer & Kraka, 1984), and the ellipticity, $\varepsilon =$

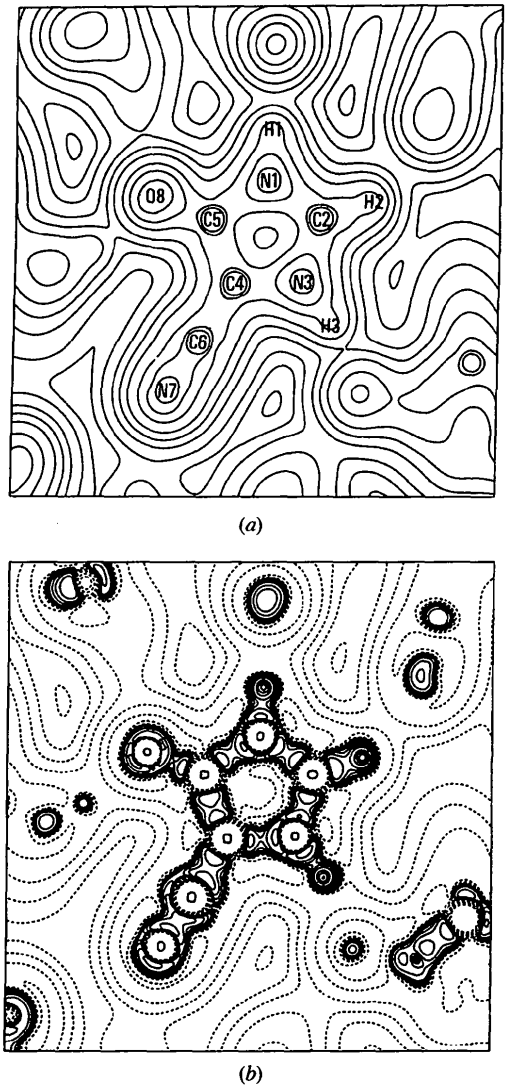

(*a*)

(*b*)

Fig. 2. (*a*) POPK electron density and (*b*) its Laplacian in the plane of molecule (1). The absolute values of contours (in a.u.) increase from the outermost one inwards in steps of 2×10^n, 4×10^n and 8×10^n with n beginning at -3 and in steps of 1. Positive values of $\nabla^2\rho$ are denoted by dashed contours, negative values by solid contours.

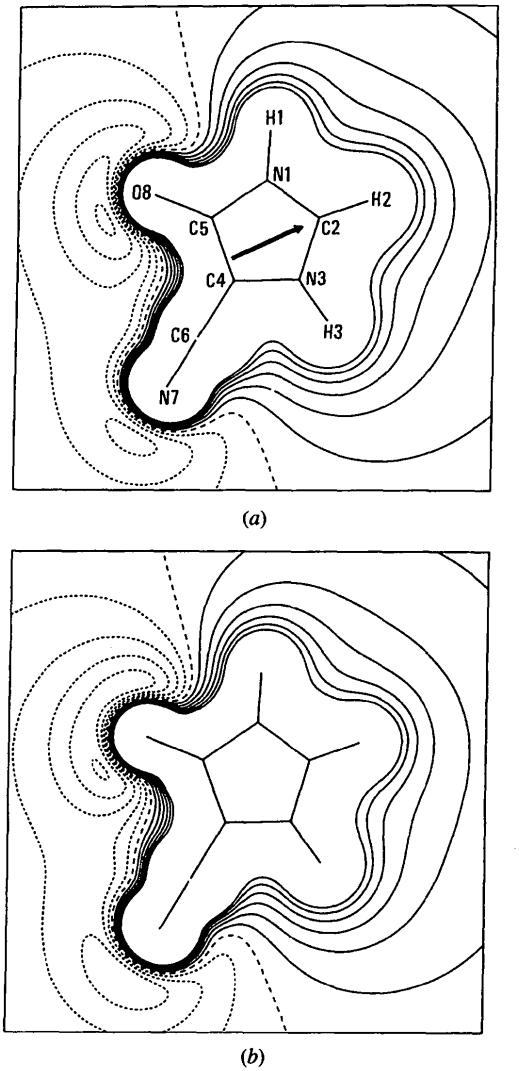

(*a*)

(*b*)

Fig. 3. (*a*) POPK multipole and (*b*) HF/6-31G** electrostatic potential maps for molecule (1). The maps are drawn in the same plane as Fig. 2. The contours are at intervals of 0.05 e Å^{-1}, the maximum level plotted is 0.30 and the minimum is -0.25 e Å^{-1}; solid lines positive, short dashed lines negative, large dashed line zero contour. (*a*) The arrow originates at the molecular center of mass and indicates the direction of the molecular dipole moment.

Table 4. *Bond critical point properties from the POPK multipole refinement*

R_x (Å) is the distance between the X atom and the BCP. The electron density, ρ_b, is in e Å^{-3} and the Laplacian, $\nabla^2\rho_b$, is in e Å^{-5}.

	Distance (Å)	R_x	ρ_b	$\nabla^2\rho_b$	λ_1	λ_2	λ_3	ε	n
Intramolecular bonds									
N1—C2	1.347	0.740	2.25 (6)	−18.9 (17)	−20.1	−14.2	15.4	0.42	1.3
N1—C5	1.396	0.806	2.03 (6)	−19.8 (18)	−17.8	−13.2	11.2	0.35	1.1
C2—N3	1.320	0.557	2.39 (7)	−26.8 (24)	−22.3	−15.9	11.4	0.40	1.5
N3—C4	1.395	0.807	2.05 (6)	−16.4 (17)	−17.5	−13.1	14.2	0.34	1.1
C4—C5	1.400	0.688	2.05 (4)	−18.6 (10)	−17.6	−12.0	11.0	0.47	1.6
C4—C6	1.397	0.709	1.98 (4)	−18.3 (15)	−15.8	−13.3	10.8	0.19	1.5
C5—O8	1.270	0.446	2.50 (10)	−31.7 (17)	−28.1	−17.6	14.0	0.60	1.6
C6—N7	1.163	0.447	3.24 (11)	−26.6 (21)	−26.1	−23.0	22.5	0.13	2.9
N1—H1	1.008	0.735	2.07 (7)	−17.6 (13)	−26.4	−24.3	33.1	0.09	
C2—H2	1.087	0.757	1.72 (5)	−15.0 (10)	−18.8	−16.6	20.4	0.13	
N3—H3	1.046	0.791	1.71 (6)	−12.1 (11)	−22.3	−20.9	31.1	0.07	
Hydrogen bonds									
H1···O8	1.773	0.629	0.23 (2)	4.0 (1)	−1.27	−1.23	6.50	0.03	
H2···N7	2.201	0.840	0.11 (1)	1.6 (1)	−0.46	−0.44	2.51	0.05	
H3···O8	1.682	0.581	0.33 (2)	4.2 (2)	−1.99	−1.97	8.15	0.01	

$\lambda_1/\lambda_2 - 1$, is a measure of the deviation of the electron density from axial symmetry. Fig. 2(*a*) shows the total electron density, $\rho(\mathbf{r})$, derived from pseudoatoms at rest in the plane containing the molecule (1). Inspection of the multipole $\sigma[\rho(\mathbf{r})]$ map in the same plane indicates that the standard uncertainty is below 0.07 e Å^{-3} in the bonding regions. The presence of saddle points related to the expected chemical interactions in the crystal structure of (1) is clearly evident in the map of Fig. 2(*a*). Fig. 2(*b*) reports the experimental Laplacian, $\nabla^2\rho(\mathbf{r})$, showing a more detailed description of the intermolecular and intramolecular interactions. Table 4 summarizes the (3,−1) BCP properties of the title compound derived from the POPK multipole model. Shared interactions (CO, CN, CC, NH and CH bonds) are correctly described by a negative value of the Laplacian at the BCP and the curvature along the bond path (λ_3) is, as expected, higher for polar than for the more covalent interactions (CC bonds). The bonds along the five-membered ring (5MR) have partial π-character and the mean of their bond orders is 1.3, close to 1.5, a typical value of Huckel aromatic compounds such as C_6H_6 or $C_3H_3^+$. However, a closer inspection of the BCP properties (Table 4) suggests that molecule (1) can be better described as the juxtaposition of two separated π-conjugated systems, linked to each other by two nearly single N—C bonds (N1—C5 and N3—C4); in fact, the latter bonds have the smallest ε and n in the 5MR. Both C5—O8 and C4—C6 interactions exhibit a significant π-character, as shown by their bond orders and ellipticities. The C—H and N—H interactions are essentially of σ-type. The N—H···O and C—H···N bonds reflect the peculiar topological characteristics of the closed-shell ionic interactions: low value of ρ_b and positive $\nabla^2\rho_b$ values with small and equal perpendicular curvatures (λ_1 and λ_2) and a dominant parallel curvature λ_3 (Table 4). It is worth noting that the BCP properties of H1···O8 (1.773 Å) are in noticeable agreement with those of H3···O2 (1.722 Å) present in the L-alanine crystal structure (Gatti *et al.*, 1992). In addition, our BCP results in the 5MR are comparable with those reported by Stewart (1991) for the imidazole crystal. These comparisons between different compounds indicate that transferability (Madson *et al.*, 1996) may also be applicable to experimental electron densities.

3.3. *Electron populations*

Experimental and Mulliken atomic electron populations are reported in Table 5. The POPK multipole model is quite close to the theoretical HF/6-31G** model. Significant differences (>3σ) are found for the N1, C2, N3, C5 and O8 atoms. The HF/6-31G** predicts that N7 and O8 atoms are more negatively charged than the POPK model. The sum of the atomic charges of 5MR and the C6 atom is −0.20 (27) and +0.19 e for the POPK and the HF/6-31G** models, respectively. Both these values are within the experimental s.u., indicating that significant negative and positive charges are essentially concentrated at opposite sites of molecule (1), forming a large dipole.

3.4. *Molecular electrostatic potential*

The overall dipole nature of the mesoionic structure is also evident in Fig. 3, a plot of the electrostatic potential for molecule (1) obtained both with the pseudoatom and HF/6-31G** models. The comparison shows good agreement between the two models; both maps present an electronegative region around CO and CN groups. This region leads to low energy or a positive test charge. A minimum of −0.25 (5) e Å^{-1} was found around the CO bond for both experimental and theoretical potentials. The negative region is differently diffused in space for the potential derived from the pseudoatom model with respect to that calculated from the *ab initio* method.

Table 5. *Atomic populations (electrons)*

	POP	POPK	HF/3-21G	HF/6-31G**
N1	7.05 (5)	7.02 (9)	7.94	7.70
C2	6.10 (7)	6.11 (17)	5.45	5.57
N3	7.13 (4)	7.20 (11)	7.89	7.64
C4	6.04 (5)	5.99 (8)	5.83	5.94
C5	6.05 (5)	6.02 (9)	5.17	5.26
C6	6.17 (6)	5.86 (10)	5.68	5.70
N7	7.06 (6)	7.28 (8)	7.53	7.48
O8	8.19 (3)	8.39 (4)	8.68	8.70
H1	0.80 (4)	0.77 (5)	0.59	0.64
H2	0.75 (6)	0.72 (9)	0.68	0.77
H3	0.64 (4)	0.63 (5)	0.57	0.62

Table 6. *Dipole moments (D)*

	POP	POPK	HF/3-21G	HF/6-31G**
μ_x	−0.8 (3)	−0.9 (4)	−1.12	−1.17
μ_y	1.4 (2)	1.7 (4)	1.71	1.73
μ_z	−0.9 (1)	−1.2 (2)	−1.17	−1.19
μ	1.8 (2)	2.3 (3)	2.35	2.40

These disagreements appear to be very likely genuine differences between crystalline and gaseous states.

3.5. *Dipole moments*

Table 6 contains the magnitudes and the components of the molecular dipole moment as calculated from pseudoatom and *ab initio* models. The difference of 0.5 e Å between the μ values derived from the two multipole models is significant on the basis of the s.u.'s. The effect of the basis set on going from the HF/3-21G to the HF/6-31G** is 0.05 e Å for the theoretical estimates of μ, but both are very close to the POPK one. In Fig. 3(*a*) the arrow, originating at the molecular center of mass, indicates the POPK dipole and it is almost exactly parallel to the plane of the figure; the center of mass being displaced by 0.01 Å from this plane. The angle between POPK and HF/6-31G** dipole estimates is ~6°.

3.6. *Energies of molecular interactions*

As we noted in the description of the crystal structure, molecules (1), stacked along *c*, are linked by hydrogen bonds, as shown in Fig. 1(*b*). An estimate of the crystal cohesive energy obtained from the model discussed above is −52 (21) kJ mol^{-1} for a cluster formed by 600 adjacent molecules. The dimer, involving hydrogen-bonded molecules (0) and (III) (Fig. 1*b*), has the largest interaction energy [−50 (10) kJ mol^{-1}]. In the dimer formed by molecules (0) and (I) the interaction energy is −38 (4) kJ mol^{-1}. This shows that the two hydrogen bonds at the O8 atom are approximately of the same strength. The interaction energy for molecules (0) and (II) is −30 (6) kJ mol^{-1}. Electrostatic interactions in this crystal structure are long range: there are pairs of molecules separated by a distance of 10.372 Å with attractive interaction energy. Other pairs of molecules, involving stacking interactions, have a strongly repulsive interaction. This is in agreement with the strongly dipolar nature of molecule (1) and the relative orientation of dipoles in the structure.

4. Conclusions

The POPK multipole model provided a quantitative description of the electron density of molecule (1), confirming its mesoionic distribution. A comparison of the BCP properties for portions of molecule (1) with the same properties in other crystals indicate a good transferability of their electron density. In the absence of complementary neutron diffraction data, the location of hydrogen positions, using the polarized H-atom model, is encouraging. The topological analysis reveals the presence of three hydrogen bonds with ionic character that contribute to stabilizing the crystal structure. Relative strengths of the hydrogen bonds at the O8 atom correlate well with H···O distances. The molecular dipole moment of molecule (1) in the crystal is very close to the theoretical calculations on an isolated molecule. The alignment of the molecules in the crystal phase does not generate a dipole-enhancing field. The next step is to investigate optical (linear and nonlinear) characteristics on the basis of ground-state electron density only.

References

Bader, R. F. W. (1990). *Atom in Molecules: A Quantum Theory.* International Series of Monographs on Chemistry 22. Oxford: Clarendon Press.

Bader, R. F. W. & Essén, H. (1984). *J. Chem. Phys.* **80**, 1943–1959.

Barni, E., Bianchi, R., Gervasio, G., Peters, A. T. & Viscardi, G. (1997). *J. Org. Chem.* **62**, 7037–7043.

Clementi, E. & Roetti, C. (1974). *At. Data Nucl. Data Tables*, **14**, 177–478.

Cremer, D. & Kraka, E. (1984). *Croat. Chim. Acta*, **57**, 1259–1281.

Frisch, M. J., Trucks, G. W., Head-Gordon, M., Gill, P. M. W., Wong, M. W., Foresman, J. B., Johnson, B. G., Schlegel, H. B., Robb, M. A., Replogle, E. S., Gomperts, R., Andres, J. L., Raghavachari, K., Binkley, J. S., Gonzalez, C., Martin, R. L., Fox, D. J., Defrees, D. J., Baker, J., Stewart, J. J. P. & Pople, J. A. (1992). *Gaussian*92. Revised. Gaussian, Inc., Pittsburgh, Pennsylvania.

Gatti, C., Bianchi, R., Destro, R. & Merati, F. (1992). *J. Mol. Struct. Theochem.* **255**, 409–433.

Hehre, W. J., Ditchfield, R., Stewart, R. F. & Pople, J. A. (1970). *J. Chem. Phys.* **51**, 2769–2773.

Johnson, C. K. (1976). *ORTEP*II. Report ORNL-5138. Oak Ridge National Laboratory, Tennessee, USA.

Madson, D., Flensburg, C. & Larsen, S. (1996). *Acta Cryst.* A**52**, C-555.

Spackman, M. A. (1986*a*). *J. Chem. Phys.* **85**, 6579–6586.

Spackman, M. A. (1986*b*). *J. Chem. Phys.* **85**, 6587–6601.

Spackman, M. A. (1987). *J. Chem. Phys.* **91**, 3179–3186.
Stewart, R. F. (1976). *Acta Cryst.* A**32**, 565–574.
Stewart, R. F. (1991). *The Application of Charge Density Research to Chemistry and Drug Design*, edited by G. A. Jeffrey and J. F. Piniella. New York: Plenum Press.
Stewart, R. F. & Spackman, M. A. (1983). *Valray User's Manual.* Department of Chemistry, Carnegie-Mellon University, Pittsburgh.
Wal, R. J. van der & Stewart, R. F. (1984). *Acta Cryst.* A**40**, 587–593.